Available online at www.sciencedirect.com
SCIENCE DIRECT®
Coordination Chemistry Reviews 249 (2005) 179–195
COORDINATION CHEMISTRY REVIEWS
www.elsevier.com/locate/ccr

Review

The use of synchrotron radiation in X-ray charge density analysis of coordination complexes

Philip Coppens [a,*], Bo Iversen [b], Finn Krebs Larsen [b]

[a] *Department of Chemistry, State University of New York at Buffalo, Natural Sciences Complex, Buffalo, NY 14260-3000, USA*
[b] *Department of Chemistry, University of Aarhus, DK-8000 Aarhus C, Denmark*

Received 2 September 2003; accepted 6 February 2004
Available online 11 May 2004

Contents

Abstract

The compelling advantages of synchrotron radiation (SR) in charge density studies of coordination complexes are described and illustrated with a number of recent synchrotron studies, ordered according to the atomic number of the metal atom involved (Cr, Fe, Cu, Zr, Mo, Th). The review concludes with two studies of the Cu-containing extended solids Cu_2O and the high-temperature superconducting phase $YBa_2Cu_3O_{6.98}$, done with very high energy synchrotron radiation of about 100 keV (~0.12 Å), very much beyond what is available at conventional X-ray sources.

Keywords: Synchrotron radiation; Coordination; Charge density; Experimental charge density; Transition metal complexes; Agnostic interaction; Extended solids

1. Introduction

As high-brightness short-wavelength synchrotron radiation (SR) is becoming increasingly accessible both in the United States and abroad, it is appropriate to draw attention to its advantages in studies beyond the determination of the atomic connectivity of compounds of which only minute microcrystals are available. Such advantages are especially pronounced when heavier atoms are present, as is the case in the field of coordination chemistry.

With bright synchrotron radiation and increasingly convenient very-low temperature devices, combined with cheap

* Corresponding author. Fax: +1-716-645-6948.
E-mail address: coppens@acsu.buffalo.edu (P. Coppens).

0010-8545/$ – see front matter © 2004 Elsevier B.V. All rights reserved.
doi:10.1016/j.ccr.2004.02.019

and abundant computing power, some of the basic assumptions of conventional crystallography can be challenged. Though charge density studies, which go beyond the assumption of element-specific spherical scattering factors, have been initially developed with conventional sources, SR offers compelling advances which are increasingly exploited. A second application, beyond the scope of this review, and rapidly gaining in importance, concerns the time-resolved study of transient species and kinetic processes.

Experimental and theoretical electron density (ED) analysis has become an attractive tool to investigate the bonding and electronic structure of metal-based compounds [1,2]. Insight into the nature of metal–ligand interactions and metal–metal bonding has been obtained, especially in the framework of the "Quantum Theory of Atoms In Molecules" (QTAIM) [3]. The physical and chemical applications range from purely organometallic systems [4], to intermetallic [5] and metallic clusters [6,7]. Such studies have been mostly restricted to first-row transition metal complexes, as anharmonic thermal motion at all but the lowest experimental temperatures complicates the analysis of heavier transition metal complexes. The use of synchrotron radiation allows measurements on very small crystal samples at short wavelengths, and thereby drastically decreases sources of uncertainty such as absorption of the X-ray beam in the crystal and rescattering of the incident and diffracted beams, processes generally referred to as multiple scattering and extinction [8]. Synchrotron radiation is tunable, and depending on the characteristics of the storage ring, often available with high intensity well beyond energies obtained at conventional sources. Wavelengths of 0.5 and 0.4 Å are widely available, thus increasing experimental resolution. And, because of the nature of the radiation, the complications in peak integration arising from the bimodal α1–α2 distribution of light emanating from X-ray tubes is completely avoided.

This review highlights the advantages of synchrotron radiation in charge density studies and a number of recent synchrotron studies of coordination complexes and metal-containing extended solids. For a broader overview of the field including results obtained with conventional sources and more detailed comparison with theoretical analyses the reader is referred to a recent review [2]. In some of the best studies experimental and theoretical approaches are combined. While the charge density is being used to extract detailed information on bonding, especially through topological analysis of the total density, and has been successfully used to obtain local energy densities through application of functionals of the electron density [9–12] it does not provide all the answers. Macchi and Sironi [13] showed that the two-electron density from theory is needed in conjunction with the one-electron density to provide a comprehensive view of the interactions of metal–metal bonding and metal–ligand bonding in a series of binuclear and polynuclear transition metal carbonyl complexes. The agreement between the experimental and theoretical charge densities in such studies attests to the level of reliability that can now be reached in accurate experimental studies and with advanced computational methods.

2. Methods of charge density analysis

Much of the earlier work was based on examination of electron density deformation maps, defined as the difference between the experimental density and the promolecule density (i.e. the density corresponding to a superposition of spherical atoms), both calculated by Fourier summation. Though the experimental electron density deformation map is thermally smeared with the internal and external modes in the crystal, it often provides excellent *qualitative* information on the system being studied, as for example in strained small ring systems, in which the bending of the bonds immediately becomes evident from accumulation of charge density outside the ring (as reviewed for both the ED deformation and the topological analysis of the charge density in [2]).

In more recent work the experimental X-ray structure factors are typically fitted with core functions and an atom-centered expansion of multipolar (spherical harmonic) valence-density functions [14,15]. The atoms as defined by the sum of the nucleus-centered multipoles are often referred to as 'pseudoatoms', and are in the Hansen Coppens formalism [15] defined by

$$\rho(\vec{r}) = \rho_{\mathrm{core}}(r) + P_{\mathrm{v}}\kappa^3\rho_{\mathrm{val}}(\kappa r) + \sum_{l=0}^{l_{\max}} \kappa'^3 R_{\mathrm{ln}}(\kappa' r) \sum_{m=0}^{+l} P_{lm\pm} d_{lm\pm}(\theta, \varphi) \quad (1)$$

where $\rho_{\mathrm{core}}(r)$ and $\rho_{\mathrm{val}}(r)$ correspond respectively to spherically averaged Hartree–Fock core and valence electron densities for isolated atoms. κ and κ' are contraction–expansion parameters and P_{v} the electron population of the corresponding atomic valence shell. Real spherical harmonics ($d_{lm\pm}$) describe the anisotropy of the valence ED through the multipole population parameters $P_{lm\pm}$. The atomic core ED $\rho_{\mathrm{core}}(r)$ is commonly fixed during the ED fitting, assuming no perturbation due to chemical bonding. The aspherical atom procedure and related interpretative routines are encoded in the XD programming package [16]. The program VALRAY [17] applied in some of the studies described below uses an essentially identical formalism.

The analytical representation defined in (1) makes it possible to plot the *static* total and deformation densities according to the model, as the thermal effects are accounted for separately in the model and can simply be omitted when the functions are plotted. Of course such maps will be affected by shortcomings in the thermal motion model, but these can be minimized by performing the experiments at the lowest possible temperatures, at which almost all modes

are reduced to zero point motion. Furthermore, as for a transition metal atom the spherical harmonic valence density functions and the d-orbital components of its wavefunction describe the same system, relations can be derived by which d-orbital occupancies are obtained from the multipole population parameters, making the well-justified assumption that overlap density in the metal–ligand bonds is small and neglecting possible asphericity of the p-orbital manifold [18].

The static model densities are now used extensively in the topological analysis of the total charge density and its Laplacian. According to the AIM theory, a direct interatomic interaction is unambiguously indicated by the existence of a bond path (line of maximum of ED), linking the two bonded atoms and characterized by the topological properties at the corresponding bond critical point (BCP, minimum of ED along the bond path). The AIM theory provides a unique decomposition of the electron density of the system in open sub-systems (the atomic basins) which are delineated by interatomic surfaces, defined by the zero-flux condition. The atomic basins are uniquely defined by the zero-flux condition in the gradient vector field of the electron density as $\vec{\nabla}\rho\cdot\vec{n} = 0$, and satisfy the quantum-mechanical virial theorem [3]. An example is given in the study of a Zr open metallocene described below (Fig. 13).

3. Charge density studies of coordination complexes

Studies of heavy element compounds are both experimentally and theoretically much more demanding than studies of organic systems. In theoretical calculations the large number of closely spaced energy levels in open shell polynuclear transition metal systems is a serious challenge. Experimentally the study of heavy elements demands more precise data, since the heavier the element, the smaller the fraction of scattering stemming from the valence electrons relative to the core contribution. Stevens and Coppens suggested a simple a priori criterion to estimate the suitability of a given crystal structure for X-ray charge density analysis [19]: $S = V_{\text{unit cell}}/\sum(N_{\text{core}}^2)$, where N_{core} is the number of core electrons of each of the atoms. The higher the suitability factor S, the more suited a given system is for experimental study by X-ray diffraction. In Fig. 1 the suitability factors for a selection of recent X-ray charge density studies are plotted against the atomic number of the heaviest element in the structures [20]. The plot is not at all comprehensive but does include studies of compounds ranging from small organic molecules to porous materials to coordination complexes. The plot nicely illustrates the challenge of coordination complexes relative to organic systems. It is, however, a testimony to the considerable increase in data quality in recent years, that it is now possible in favourable cases to study systems containing even thorium atoms ($Z = 90$). We discuss a number of examples of synchrotron charge density studies of metal complexes, ordered according to the atomic number of the metal atom involved

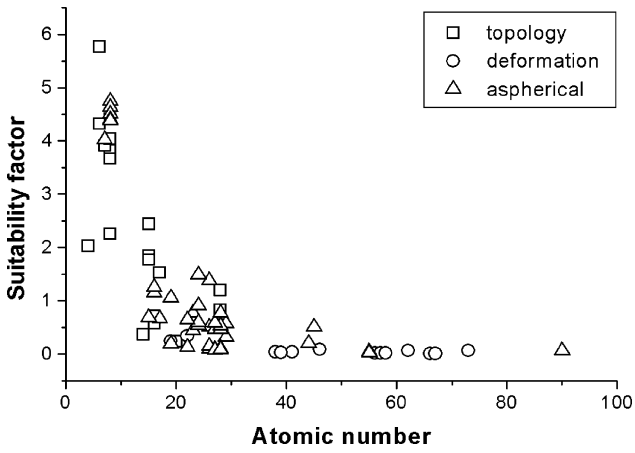

Fig. 1. The suitability factor vs. the atomic number of the heaviest atom in the corresponding structure for a selection of X-ray charge density studies. Squares represent studies employing topological analysis, triangles studies employing aspherical modeling, circles experimental deformation density studies.

(Cr, Fe, Cu, Zr, Mo, Th), and conclude with two studies of Cu-containing extended solids done with very high energy synchrotron radiation of about 100 keV, very much beyond what is available at conventional X-ray sources.

3.1. Host–guest chemistry in a large polynuclear cluster

One of the largest molecules studied so far with X-ray charge density methods is the octanuclear chromium cluster $[Cr_8F_8(tBuCO_2)_{16}]$ [21] (Fig. 2) which contains 272 unique

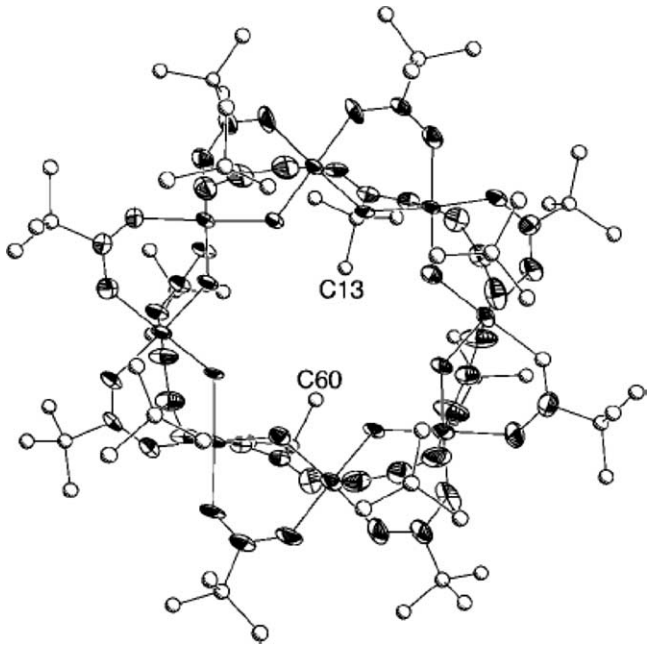

Fig. 2. ORTEP-drawing of $[Cr_8F_8(tBuCO_2)_{16}]$ viewed along the normal to the chromium-wheel molecular plane. Ellipsoids truncated at the 50% probability level. Positions of all Cr and F atoms of the $[Cr_8F_8Piv_{16}]$ molecule are indicated as are C and O atoms of the 16 coordinating pivalate groups. Reprinted with permission from ref. [21]. Copyright of the Wiley-VCH Verlag GmbH & Co.

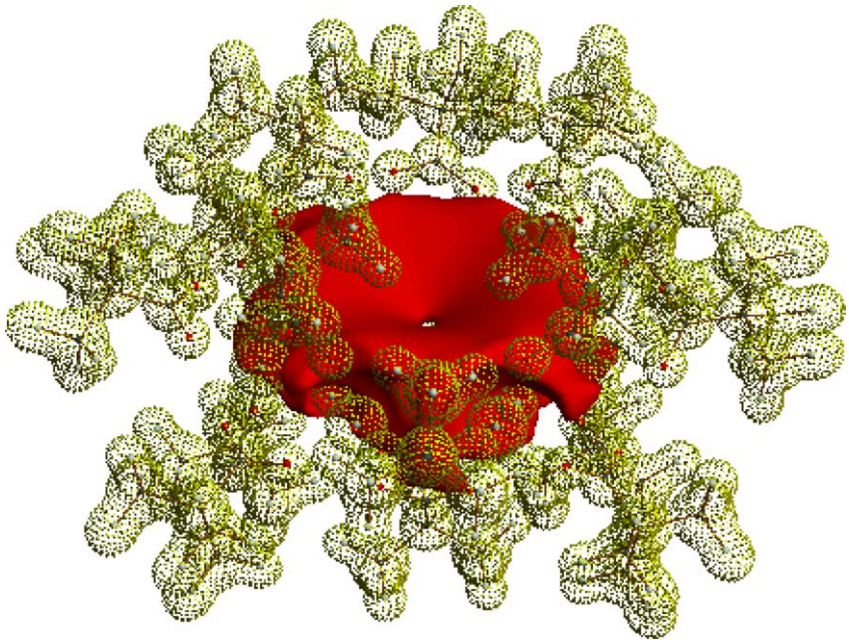

Fig. 3. Isosurface plot of the electrostatic potential in $[Cr_8F_8(tBuCO_2)_{16}]$. Surface at $-0.54\,e\,Å^{-1}$ (red) and $+0.3\,e\,Å^{-1}$ (yellow). Reprinted with permission from ref. [21]. Copyright of the Wiley-VCH Verlag GmbH & Co. (For interpretation of the references to color in this figure legend, the reader is referred to the web version of the article.)

atoms (1144 e^-) in a 23327(9) $Å^3$ unit cell. Supramolecular inclusion chemistry is a rapidly expanding field of increasing importance in both basic science and technology [22,23]. The properties displayed by host molecules at the binding site(s) for the guest molecules are controlled by the accessibility and shape and size of the cavity as well as the electrostatic environment. Determination of the geometry of the host structure has been accomplished by from X-ray crystallographic investigations [24], whereas the (electrostatic) interactions between host and guest molecules have been estimated mainly from speculations based on the known polarity of the relevant functional groups or from theoretical calculations [25]. It is clearly desirable to obtain information about the electrostatic potential of host molecules in order to be able to predict properties conducive for the acceptance of guest molecules.

Apart from the interest in the host–guest chemistry, high nuclearity cluster molecules have also attracted large interest as potential single molecule magnets. The present Cr_8 molecule is antiferromagnetically coupled and characterised by an $S = 0$ ground state [26], and thus has no use in magnetic applications. However, the molecule is used as starting point for further molecular engineering [56].

In Fig. 3, the electrostatic potential of the naked host molecule is shown as determined from the multipole modelling of 16 K synchrotron data. A three-dimensional saddle point in the electrostatic potential is located at the molecular center with a minimum along the axis perpendicular to the Cr_8-plane and a maximum within this plane. The local character of the positive isosurfaces shows that the electrophilic regions are closely confined to the methyl groups on the outside of the molecule. The negative region of the potential hardly protrudes out of the cavity entrance on the 'open' side of the molecule. The first negative contour shown ($-0.1\,e\,Å^{-1}$) extends outside the 'open' side, whereas this contour is within the molecule on the opposite side. In the molecular cavity, the negative potential reaches a local minimum along the molecular axis at the center with a value of $-1.24\,e\,Å^{-1}$. The central potential is quite flat and the area of negative potential within 5% of the center value spans a circular area with a radius of more than 2 Å.

From the electrostatic potential it is clear that guest molecules have to be oriented quite specifically for inclusion to occur, since positive guest entities will be repelled by the outer molecular envelope, before they attain stabilisation in the center. Thus, there must be a considerable barrier for inclusion. On the other hand, the weakness of the inclusion capabilities may be used for selectivity because only a limited number of small molecules can be bound inside the cavity. An extended linear molecule with a permanent dipole will be able to stabilize both ends of the molecule by being placed asymmetrically out of the molecule, i.e. the positive end inside the cavity and the negative end outside the cavity. It is not favorable to place a permanent dipole totally inside the host (i.e. symmetric inclusion across the molecular center). From the electrostatic potential it is predicted that neutral molecules only will be weakly bound, whereas one dimensional molecules (chains) having a permanent dipole moment can be stabilized asymmetrically. Small positive cations can be stabilized in the molecular cavity, but crystallisation of such host–guest complexes has not been possible, and they only appear in the liquid and

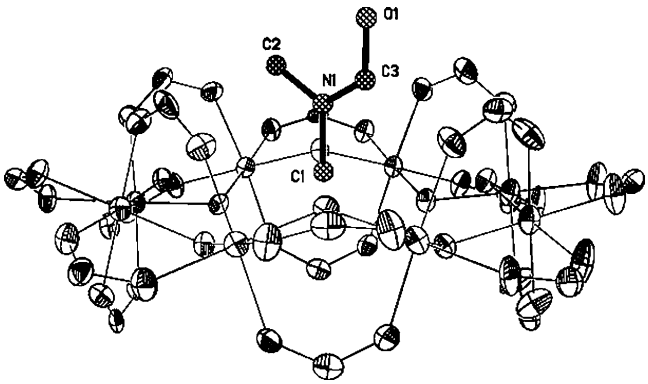

Fig. 4. ORTEP-drawing showing the position of dimethylformamide inside the cavity of the chromium-wheel in the complex. The chromium-wheel molecular plane is viewed side-on and the *t*-butyl part of the 16 coordinating pivalate groups have been omitted from the drawing to expose better the position of the guest molecule. Reprinted with permission from ref. [21]. Copyright of the Wiley-VCH Verlag GmbH & Co.

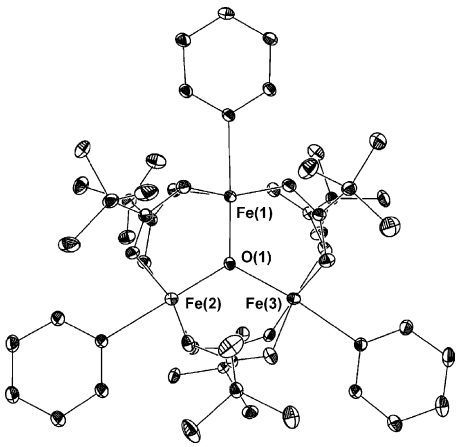

Fig. 5. Structure of $[Fe_3O(OOCC(CH_3)_3)_6(C_5H_5N)_3]$ at 28 K. Reprinted with permission from ref. [32]. Copyright of the American Chemical Society.

the gas phase [52]. Negative ions may be able to associate with the outer envelope of the molecule. The predictions of inclusion properties were tested by synthesis of host–guest complexes with different guest molecules. As an example the inclusion of dimethylformamide is observed with the electrophilic methyl groups stabilized in the center of the cavity and the nucleophilic oxygen extending outside the molecule to obtain stabilization from the positive potential regions on the molecular surface (Fig. 4).

The electron density analysis of the cluster shows expected trends. The experimentally derived orbital populations on the Cr atoms are 0.91(5) and 0.71(5) for d_{z^2} and $d_{x^2-y^2}$ (destabilized e_g orbitals), and 1.51(5), 1.00(5) and 1.32(5) for d[*xy*], d[*yz*], d[*xz*], respectively (stabilized t_{2g} orbitals). These values are similar to values obtained in studies of $Cr(CN)_6^{3-}$ and $Cr(CO)_6$ [27]. It is encouraging that the experimental density obtained by synchrotron radiation measurements on a huge molecule like $[Cr_8F_8(tBuCO_2)_{16}]$ can be quite accurate. Comparative quality theoretical calculations on a molecule of this size are very demanding even if based on the experimental geometry.

3.2. Redox active polynuclear transition metal complexes

Redox active mixed valence (MV) polynuclear transition metal centers are involved in many biological electron transfer (ET) processes [28]. In enzymes, the transition metal atoms at the active sites are often linked by oxo, hydroxy or water bridges. A large number of studies have attempted to synthesize model complexes with similar properties as possessed by proteins [29]. The trinuclear iron carboxylates, $[Fe^{III}{}_2Fe^{II}O(O_2CR_3)_6L_3]\cdot nS$,[1] are among the most studied classes of MV model compounds due to their relative simplicity, their potential use as oxidation catalysts and their many interesting physical properties [30]. The compound $[Fe_3O(O_2CC(CH_3)_3)_6(C_5H_5N)_3]$ (Fig. 5) was found to exhibit extraordinary temperature dependent changes of the central Fe–μ^3–O bond lengths [31], as shown in Fig. 6.

Since the complex is neutral, there are formally at any time two Fe atoms of valence III and one Fe atom of valence II. At room temperature the structure is observed to have one Fe–μ^3–O bond length typical of $Fe^{(III)}$ and two Fe–μ^3–O bond lengths that are intermediate between $Fe^{(III)}$ and $Fe^{(II)}$ values. However, below 35 K the structure becomes valence trapped and contains two $Fe^{(III)}$–μ^3–O and one $Fe^{(II)}$–μ^3–O bonds. The intramolecular ET process only involves two of the metal sites, Fe(2) and Fe(3), with Fe(1) being valence trapped at all temperatures.

The 28 K synchrotron charge density of the complex provides novel insight in trinuclear carboxylate complexes [32]. In this case much of the analysis is based on the Laplacian of the total charge density, defined as $\nabla^2(\rho)$, the sum of the diagonal elements of the Hessian matrix. The

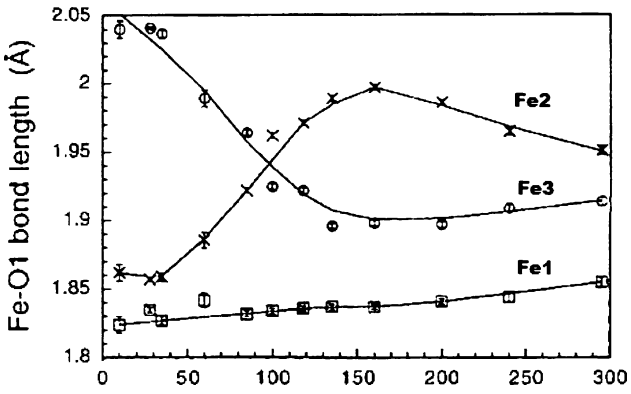

Fig. 6. The variation of the central Fe–O bond lengths in $[Fe_3O(OOCC(CH_3)_3)_6(C_5H_5N)_3]$ with temperature. Reprinted with permission from ref. [31a]. Copyright of the American Chemical Society.

[1] O_2CR designates substituted carboxylate bridges, L terminal ligands and S solvates.

Laplacian shows minima in regions of charge concentration, and maxima where charge is depleted. Contrary to expectations based on the geometry (planar Fe_3O core) three bonded valence shell charge concentration (VSCC) maxima in the Fe_3O plane are not observed. While Fe(1) and Fe(3) have the expected s-interaction with an oxygen VSCC, as shown in Fig. 7a and c, Fe(2) interacts with two VSCC maxima of μ^3–O above and below the plane (Fig. 7b). The effect is seen both in the deformation maps and in plots of the Laplacian distribution. The same study [32] also includes charge density analyses of two other Fe_3O complexes, $[Fe_3O(CH_2ClCOO)_6(H_2O)_3]\cdot 3H_2O$, and the oxidized form of this complex, $[Fe_3O(CH_2ClCOO)_6(H_2O)_2(CH_2ClCOO)]\cdot 1H_2O$. The surprising sp^3-like feature on the central oxygen atom is also found in the other mixed valence complex, $[Fe_3O(CH_2ClCOO)_6(H_2O)_3]\cdot 3H_2O$, but not in the oxidized form. It therefore appears to be a fingerprint of the mixed valence state.

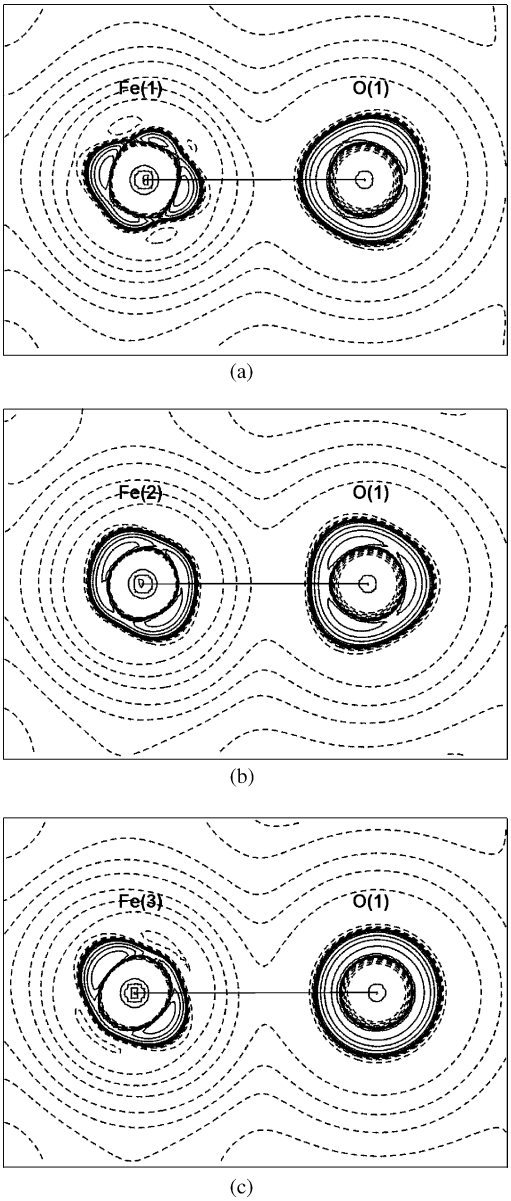

Fig. 7. Laplacian maps ($\nabla^2(\rho)$) in the bonding planes perpendicular to the Fe_3O plane in $[Fe_3O(OOCC(CH_3)_3)_6(C_5H_5N)_3]$. Contours at ± 2, 4, 8×10^n e Å^{-5}, $n = -3, -2, -1, 0, 1, 2$. Solid lines are negative contours, dashed lines are positive. Reprinted with permission from ref. [32]. Copyright of the American Chemical Society.

Analysis of the d-orbital populations on the metal sites [18] in the three complexes provides other important information on the electron transfer process. Comparison between the mixed valence and the oxidized complexes shows that the extra electron density on the Fe^{II} site primarily is distributed in a d(*yz*) orbital (*z*-axis towards the central oxygen, *y*-axis perpendicular to the Fe_3O-plane). This means that it is mostly d(*yz*) electron density which is transferred between the metal centers. The analysis furthermore reveals that presence of extra charge in the d(*yz*) orbital correlates with a decrease in the d(*xy*) population, i.e. with a depletion of charge in the equatorial region of coordination to carboxylate oxygen. The d(*xy*) charge depletion appears to be of importance for determining the active versus trapped Fe^{III} site, and the equatorial ligands therefore have a considerable influence on the ET process.

The direct comparison between ground state densities on three similar complexes thus reveals information which cannot be deduced from a single density, and is related to electron migration in a chemical process rather than just ground state properties. In this generalised structure-correlation study the comparison and correlation of bond lengths and angles in related structures has been taken one step further to the charge density level.

3.3. α-Diaqua bis(hydrogenphthalate) copper(II): a compound with a very short asymmetrical hydrogen bond and essentially square planar Cu coordination

The charge density of α-diaqua bis(hydrogenphthalate) copper(II) (Fig. 8), [33] was determined at 17 K with

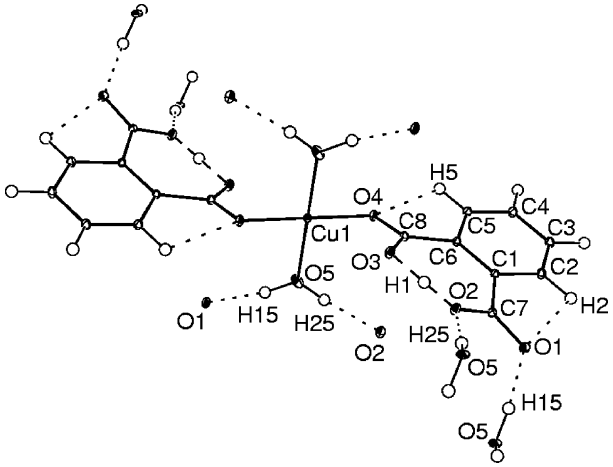

Fig. 8. Ortep drawing of α-diaqua bis(hydrogenphthalate) copper(II) at 17 K showing the inter and intramolecular hydrogen bonds (dashed lines). The ellipsoids correspond to 50% probability.

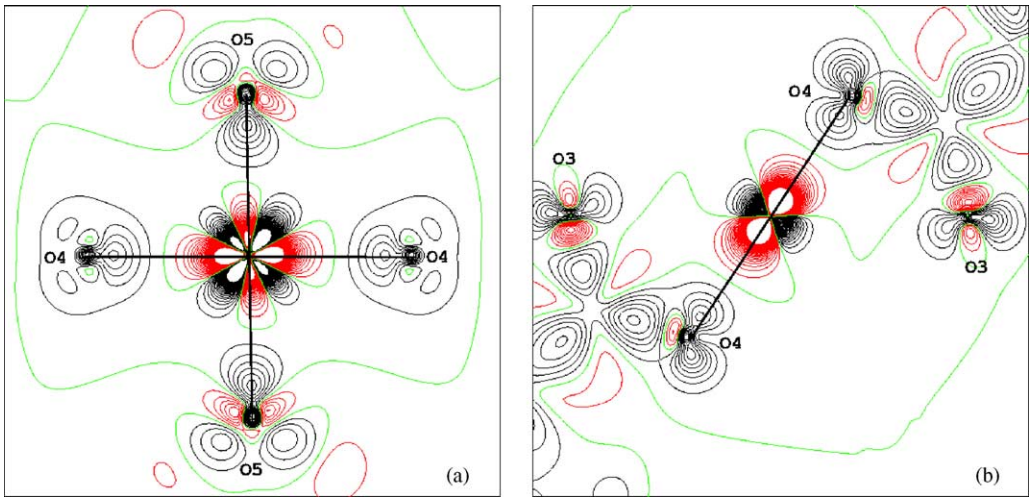

Fig. 9. Deformation density maps in the planes (a) O4–Cu–O5 (the *xy* plane) and (b) O3–Cu–O4 (the *xz* plane) of α-diaqua bis(hydrogenphthalate) copper(II). Contour levels each 0.10 e Å^{-3}. Black: positive contours; red: negative contours; green: zero level. (For interpretation of the references to color in this figure legend, the reader is referred to the web version of the article.)

short-wavelength ($\lambda = 0.394$ Å) synchrotron data, collected up to the limit of $\sin(\theta/\lambda) \leq 1.55$ Å^{-1}.

The copper atom in the complex has an elongated distorted octahedral coordination, with the axial oxygen at 2.629(2) Å, compared with 1.928(1) and 1.950(1) Å for the equatorial oxygen atoms. The angle between axial Cu–O and the equatorial plane is only of 54.3°. The study was aimed at elucidating influence of the distorted coordination on the electron density and at the nature of the very short but asymmetric hydrogen bond (not further discussed here) in the phthalate ligand.

The deformation density around the Cu atom in the basal plane shows the classic preference for density accumulation in the regions away from the ligand atoms (Fig. 9a). No such deficiency is observed towards the more remote O(4) atom. This result indicate a square planar, rather than an octahedral coordination of copper. In agreement with the density maps, the Cu d-orbital occupancies derived from the multipole population parameters show the d[$x^2 - y^2$] orbital, directed to the equatorial ligands (O4 and O5) to be less occupied and the d[*xy*] orbital, directed bisecting the vectors Cu–O4 and Cu–O5, to be more occupied than would be the case in the spherically averaged atom, while the d[z^2] orbital is slightly overpopulated, in accordance with predictions of crystal field theory for a square planar coordination. The difference in population of the d[*xz*] and d[*yz*] orbital is likely related to the presence of oxygen O3 in the *xz* plane, even though it is located considerably farther from the central Cu atoms than the other oxygen atoms.

A density functional theory (DFT) calculation with the B3LYP functional, was performed with Gaussian 98 [34] and the 6-311G** basis sets were used for C, N and O, and Lanl2dz for Cu. The resulting d-orbital populations (Table 1) with preferential occupancy of d[*xy*] and to a lesser extent d[z^2]. The d[$x^2 - y^2$] orbital is less populated than it would be for a spherical distribution, though the difference between the d[*xy*] and d[$x^2 - y^2$] orbital populations is somewhat less than observed experimentally. In contrast with the experimental results, the d[*xz*] and d[*yz*] populations are almost equal according to the calculation. Nevertheless, the agreement, especially regarding the pronounced depopulation of the d[$x^2 - y^2$] orbital is quite satisfactory, as some differences may be expected given solid state effects and approximations in both theory and experiment.

3.4. Agostic interaction in an open zirconocene

Metal pentadienyl compounds display a great deal of diversity in their structural nature as well as a rich variety of reaction chemistry, including coupling reactions, applications in metal film depositions, syntheses of new materials, and catalysis [35]. Studies of open and half-open titanocenes and zirconocenes have demonstrated that pentadienyl li-

Table 1
Populations of 3d orbitals of copper atom in α-diaqua bis(hydrogenphthalate) copper(II) from multipole refinement and quantum-mechanical calculation

	d[$x^2 - y^2$]	d[z^2]	d[*xy*]	d[*xz*]	d[*yz*]	Total
Experiment	1.00 (10.8%)	1.93 (20.7%)	2.38 (25.7%)	1.73 (18.6%)	2.24 (24.2%)	9.28
Theory 6-311G**	1.310 (14.1%)	1.969 (21.2%)	1.994 (21.5%)	1.991 (21.5%)	2.002 (21.6%)	9.27

The lower population of d[*xz*] relative to d[*yz*] according to experiment, but not to theory, is likely related to the presence of O(3) in this quadrant. The total d-orbital populations on Cu show very good agreement between theory and experiment.

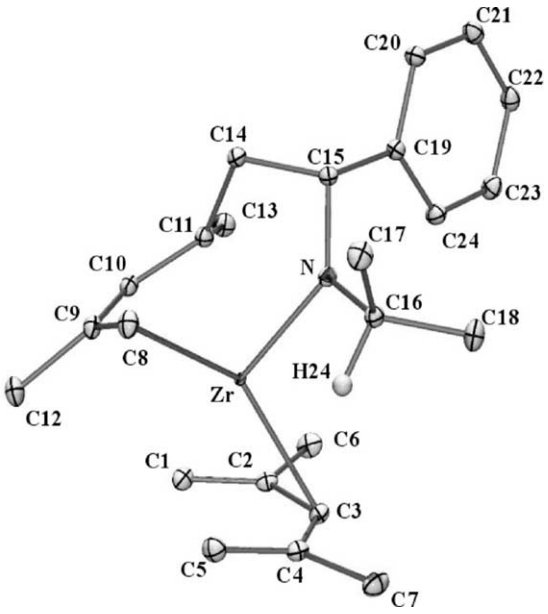

Fig. 10. ORTEP drawing of Zr(2,4-C_7H_{11})[(iPr)NCHPhCH_2Cme=CHCMe =CH_2] Reprinted with permission from ref. [45]. Copyright of the American Chemical Society.

gands may be both more strongly bound and more reactive than their cyclopentadienyl counterparts [36–38].

Based on evidence from C–C bond lengths, reduced ^{13}C-^{13}C coupling constants, and supporting theoretical studies, agostic interactions have been proposed to play a role in the metal–ligand interactions [39]. In Zr(2,4-C_7H_{11})[(iPr)NCHPhCH_2CMe=CHCMe=CH_2] (C_7H_{11}: dimethylpentadienyl) (Fig. 10) the Zr–N–C–H group has the unusually small Zr–N–C angle of 102.87(4)°, compared to a value of 130.4(4)° in a similar titanium complex [40]. Nevertheless, the C–H coupling constant of ca. 125 Hz. does not seem to support a (C-H)···Zr interaction. As the nature of the bonding in various agostic and σ-bond complexes is directly and fundamentally related to the oxidative addition process [41,42], and to many other types of bond activation reactions [43] an understanding of the interactions involved is of importance. A study with a conventional source [44] on the agostic interaction in the titanium complex [EtTiCl3(dmpe)][(dmpe) 1,2-bis-(dimethylphosphino)ethane] provided evidence for the existence of bond paths corresponding to both the Ti···Cα and Ti···Hβ interactions, though the proximity of the Ti···Hβ bond critical point to a ring critical point in the complex indicates the weakness of the interaction.

The charge density study of Zr(2,4-C_7H_{11})[(iPr)NCHPh-CH_2CMe=CHCMe=CH_2] gives detailed insight into the nature of the bonding interactions [45]. The deformation of the valence ED around the zirconium atom and in two of the ligand planes is illustrated in Fig. 11 while a 3D representation is given in Fig. 12. Two kidney-shape lobes of positive deformation density are directed towards the conjugated systems of both ligands (maximum of 0.6 e Å^{-3}), and four negative lobes (minimum of −0.5 e Å^{-3}) are located in the perpendicular plane. The local coordinate system for Zr has been chosen according to these directions, assuming the *z*-axis along the positive lobes and the *x*-axis pointing towards the nitrogen atom. The positive lobes correspond to an increase of the $4d_{z^2}$ orbital population with regards to the isolated zirconium atom (taking the $5s^2 4d^2$ valence state as reference), whereas the negative lobes indicate a depopulation of the $4d_{xy}$ atomic orbital. The kidney shape of the positive lobes results from the enediyl coordination mode, which elongates the deformation density in the Zr-C8-C11 plane. The Zr 4d-orbital populations, derived from the multipolar expansion of the deformation density [46], differ slightly depending on whether or not 5s electrons, which are very diffuse and therefore scatter only in the very-low order region, are included in the treatment. A representative example of the results is given in Table 2.

Table 2
Zr d-electron populations in Zr(2,4-C_7H_{11})[(iPr)NCHPhCH_2CMe=CHCMe=CH_2]

d[$x^2 - y^2$]	0.46(3)
d[z^2]	0.72(3)
d[*xy*]	0.05(3)
d[*xz*]	0.69(3)
d[*yz*]	0.003(3)
Total	1.92(7)

The atomic and fragment charges from numerical integration over the atomic basins [45] indicate a charge transfer of 2.16 e from the Zr atom to the ligands, in good agreement with the d-orbital popualtion analysis. The tranferred charge is more localized on the $C_{17}NH_{24}$ ligand (1.48 e) than on dimethylpentadienyl (0.68 e). The N atom has a considerable charge of −1.05 e indicating high electrostatic Zr–N interactions in addition to the σ–π N → Zr donations into the d_{xz} orbital. Bader et al. [47] report a high charge transfer of "approximately 3 e" from Ti to cyclopentadienyl and diene fragments in a similar complex.

No bond paths are found connecting Zr···H24 or Zr···C16 (Fig. 13). There also is no apparent curvature in the Zr–N bond path, whereas at least in β-agostic alkyl complexes, bent M–C bond paths have been observed [44]. The atomic charge obtained by numerical integration over the atomic basin for H24 is positive (+0.05), as opposed to what had been observed by Popelier in a calculation on the α-agostic CH_3TiCl_2 cation [48]; this positive charge would be consistent with a primarily sigma (donation) interaction.

According to (C···H)–M distance criteria defined by Crabtree et al. [49] the geometry in the Zr complex is indicative of a metal–C–H interaction, while the M–H–C angle is calculated as 94.32(3)°, again in a typical range for accepted agostic interactions. Nevertheless, overall the ED results do not support the existence of an agostic bridge, notwithstanding the small Zr–N–C angle.

While the results do not explicitly establish what sort of interaction is responsible for the small Zr–N–C angle, it is worthwhile to quote Popelier [48] on the rotation of the

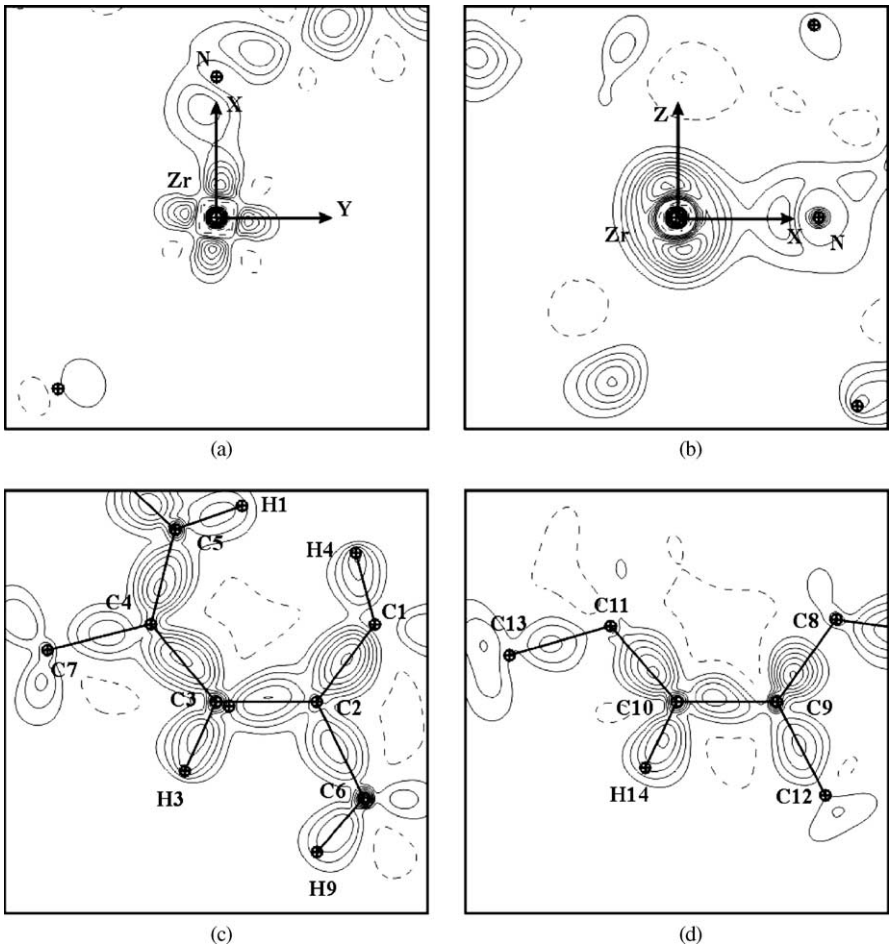

Fig. 11. Static deformation density in planes through Zr and the ligand atoms in Zr(2,4-C_7H_{11})[(iPr)NCHPhCH$_2$CMe=CHCMe=CH$_2$]. (a) The *xy* plane of Zr, (b) the *xz* plane of Zr, (c) the dimethylpentadienyl ligand and (d) the butadiene fragment. In (b) N atom is out of the plane. Contour interval 0.1 e Å^{-3}, positive contours are solid lines, and negative contours dashed lines. The coordinate system is shown in Fig. 12. Reprinted with permission from ref. [45]. Copyright of the American Chemical Society.

methyl group in the CH_3TiCl_2 cation: "In going from the staggered to the eclipsed conformation the C–H_3 bond becomes longer, the Ti–C–H_3 angle reduces to almost 90°, the ρ_b value is reduced and the electron population of H_3 increases. These effects are collectively reminiscent of the formation of an agostic bond (potentially between Ti and H_3) although there is clearly no BCP present. So although both geometrical effects and AIM properties point in the direction of α-agostic interaction, we do not find a bond expressing this interaction". Furthermore, in the Ti(C_2H_5)Cl_3(dmpe) complex an extremely flat gradient path was observed, leading to the conclusion that bond critical points may not always be observed for agostic interactions [44]. The discrepancy between ED results and the observed geometric distortions merits further attention if a proper understanding of agostic interactions is to be obtained.

3.5. Transition metal epoxidation

The first experimental ED study to include topological analysis on a system beyond the first transition series was a synchrotron radiation study of the oxidation catalyst oxoperoxo(pyridine-2,6-dicarboxylato)(hexamethylphosphoramide) molybdenum(VI), (MoO_3(dipic)(HMPA)), Fig. 14 [50]. The chemistry of dioxygen transition metal complexes is a very active field of research, and the structure and chemical bonding of dioxygen transition metal complexes has been studied in considerable detail [51]. The extensive interest in dioxygen complexes stems from the large number of applications of the compounds, including industrial processes [52]. One of the most important reactions is epoxidation of olefins by peroxo complexes. The mechanistic aspects of olefin epoxidations have recently attracted renewed interest from both theoreticians and experimentalists [53]. Two main hypotheses have dominated the discussions. The first is due to Mimoun, who suggested that the olefin coordinates to the metal center before subsequent insertion into the Mo–O bond to form a five-member metallacycle [54]. Sharpless suggested a concerted reaction mechanism involving a direct attack by the olefin on the peroxo oxygen atoms (with a three member ring intermediate) [55]. Qualitatively, the basic difference between the two proposals in

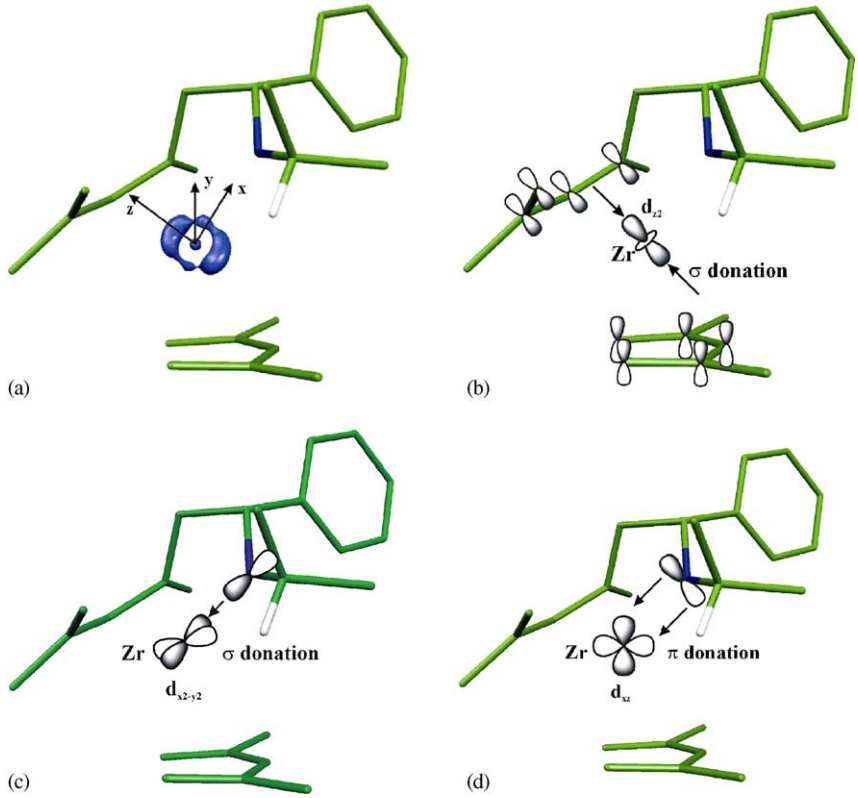

Fig. 12. Three-dimensional representation of (a) the static deformation density around Zr atom for model III and schematic representation of the (b) Zr ← diene σ donation, (c) Zr ← N σ donation and (d) Zr ← N π donation. Isocontour of 0.2 e Å^{-3} (positive in blue). Reprinted with permission from ref. [45]. Copyright of the American Chemical Society. (For interpretation of the references to color in this figure legend, the reader is referred to the web version of the article.)

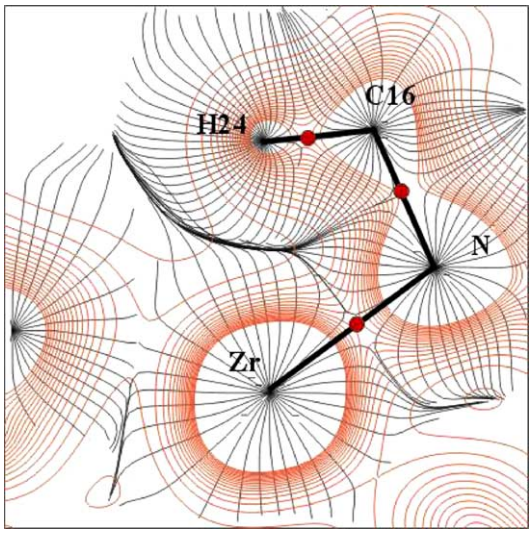

Fig. 13. Gradient trajectories (black lines) and total electron density (red lines) in the Zr-N-C16-H24 plane. Bond CPs are depicted as red circles. Contour levels at 0.1 e Å^{-3}. The gradient trajectories are computed in a slice and projected on the plane of the figure, so that some of them appear to cross each other. Reprinted with permission from ref. [45]. Copyright of the American Chemical Society. (For interpretation of the references to color in this figure legend, the reader is referred to the web version of the article.)

charge density terms, is which group, i.e. the olefin or the peroxo group, has undergone a reversal of the polarity. In the Mimoun mechanism coordination of the olefin to the metal center (either substitution or addition) is thought to cause an electron flow from the olefin to the metal. This

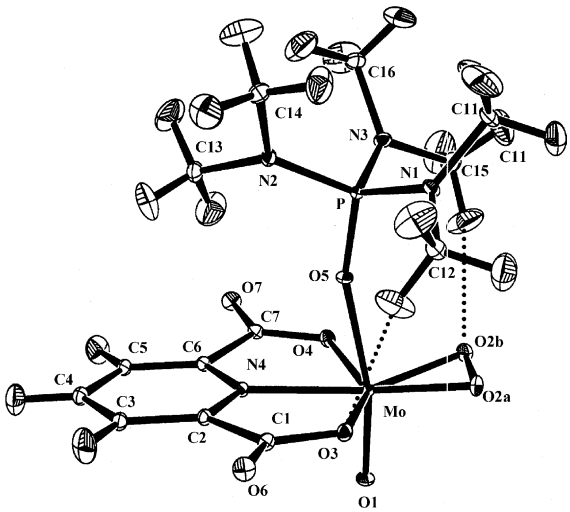

Fig. 14. Molecular structure of oxoperoxo(pyridine-2,6-dicarboxylato) (hexa-methylphosphoramide)molybdenum(VI) at 20 K. Reprinted with permission from ref. [50]. Copyright of the American Chemical Society.

makes the olefin electrophilic [56] and ready for further reaction with the peroxo group acting as a nucleophile. In the Sharpless mechanism, it is the coordinated peroxo group that undergoes "umpolung" to decrease the negative charge and increase its electrophilic character. The reversed polarity makes the peroxo oxygens susceptible to direct reaction with the electron rich double bond of the olefin.

The study of transition metal epoxidation exemplified by MoO_3(dipic)(HMPA) concerned three main issues: (i) structural correlation based on known crystal structures of Mo-peroxo complexes, (ii) theoretical modeling of prototype molecules containing peroxo groups, and (iii) experimental and theoretical charge density analysis of MoO_3(dipic)(HMPA). The structure analysis and the theoretical modeling of prototype complexes revealed that some organic peroxo functions (especially dioxiranes) have a pronounced reversal of polarity resulting in a substantial electrophilic character, while transition metal peroxides only have an intermediate electrophilicity, somewhat similar to H_2O_2.

The experimental charge density study of MoO_3(dipic)(HMPA) was based on combined analysis of 20 K synchrotron X-ray and 20 K neutron diffraction data. The ED analysis documented that the Mo–O_{peroxo} bond contains considerable covalent character with a short Mo–O distance, a large ED along the bond path, and a negative energy density at the bond critical point (bcp). The O–O distance, the atomic charges and the electrostatic potential around the peroxo group are different from those of dioxiranes (Fig. 15). In terms of reactivity, transition metal peroxides are therefore expected to be less prompt in undergoing a classical S_N2-type reaction. In reactions with olefins a further re-polarization is necessary either of the M–(O_2) group or of the C=C group. It is impossible to deduce a mechanism for transition metal epoxidation based only on knowledge of the initial state ED, but the analysis of the ED establishes the electronic and electrostatic requirements for a given mechanism to take place. Thus, there are clear differences between transition metal peroxo functions and dioxiranes, whose peroxo function is readily available for nucleophilic attack. The study of MoO_3(dipic)(HMPA) shows that X-ray charge density analysis is a promising tool in coordination chemistry not only for investigation of bonding types and molecular properties, but also indirectly for understanding of chemical reactivity.

3.6. The charge density of $Th(S_2P(CH_3)_2)_4$—going to the limit

The first sub-liquid nitrogen temperature synchrotron ED study was on $Th(S_2PMe_2)_4$ [57] (Fig. 16) in which novel low-temperature equipment was employed [58]. This compound is a quite unusual candidate for an experimental or theoretical ED study. Quantitative electronic information for actinide compounds is scarce, since theory has problems treating very relativistic systems, and in the X-ray experiment bonding information gets swamped by the scattering of the heavy actinide core. The X-ray study of $Th(S_2PMe_2)_4$ was possible since the crystal structure is unusually simple and symmetrical for a heavy metal complex [59]. Furthermore, due to the site symmetry of the Th atom, one half of the reflections contain *no* contribution from the extremely electron-rich thorium core.

In studies of compounds with such very heavy elements, it is vital to use intense, short-wavelength synchrotron radiation and very small crystals (<80 μm) to reduce absorption and anomalous scattering for the reasons discussed above. Another important issue in experimental ED studies of heavy atom compounds is the separation of anharmonic thermal motion from aspherical bonding effects. The problem is particularly serious for heavy element compounds since electron deformation due to preferential occupancy of the metal valence orbitals is typically located quite close to the nuclei. In organic molecules the redistribution of charge upon bonding involves the mid-bond regions between atoms, and the atoms involved have fewer electrons, leading to smaller

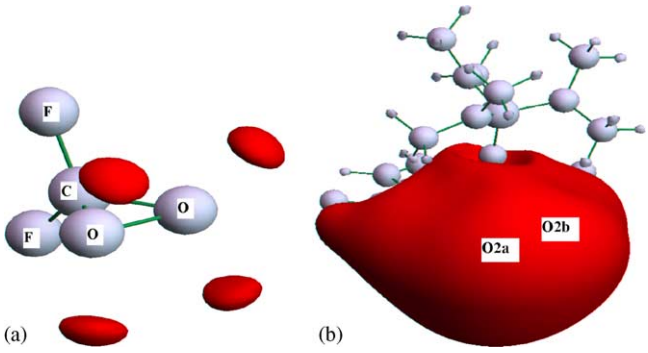

Fig. 15. Negative electrostatic potential for (a) F_2CO_2 (dioxirane, theoretical calculation), and (b) Mo(O_2)O(HMPA)(dipic) (derived from experimental data). The iso-surfaces represent negative $\phi(r)$ ($= -0.03\,e\,Å^{-1}$) in (a); ($= -0.1\,e\,Å^{-1}$) in (b); atomic nuclei are represented with light spheres. For atomic labeling see Fig. 14. Reprinted with permission from ref. [50]. Copyright of the American Chemical Society.

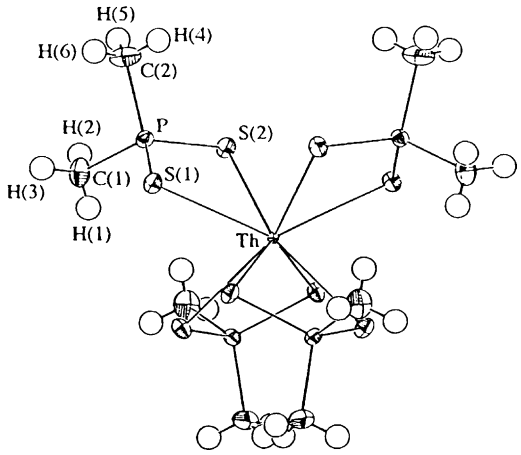

Fig. 16. Molecular structure of $Th(S_2PMe_2)_4$ at 28 K. Reprinted with permission from ref. [57a]. Copyright of the American Chemical Society.

correlation between electronic and thermal parameters. Restori and Schwarzenbach [60] have argued that anharmonic motion and electron deformation bonding effects are not practically separable with use of X-ray data at a single temperature only, as the symmetry of the anharmonic thermal motion probability functions and the spherical harmonics used to describe the asphericity of the density are identical. However, their radial dependences are different, with thermal motion affecting especially the high-order reflections and valence electron scattering being concentrated in the small-angle low-order region. Mallinson et al. have shown in a model calculation on theoretical structure factors on the low-spin $Fe(H_2O)_6^{2+}$ ion and in a refinement of experimental data on bis(pyridine)(*meso*-tetraphenylporphinato)iron(II) that with accurate data and careful refinement the two effects can be separated [61].

The definition of nuclear motion can be achieved independently in a parallel neutron diffraction experiment, or several X-ray datasets at different temperatures. X-ray data sets at different temperatures can be used because electron deformation parameters are in general independent of temperature, while thermal vibrations have distinct temperature dependence.

In the study of $Th(S_2PMe_2)_4$ it was possible to separate anharmonicity and electron deformation from a single X-ray data set. This was due to the unusual high accuracy of the synchrotron data, which also extended to very high order (1.80 $Å^{-1}$), possible because of excellent crystal quality, use of very hard $\lambda = 0.39$ Å radiation and data collection at very-low temperature (28 K). Furthermore, the heavy thorium core is quite non-Gaussian, which gives less correlation with the Gaussian temperature factor in the least squares refinement. Such extensive data cannot be expected in general, and in cases where the anharmonicity is large, unbiased neutron data may be required to convincingly separate anharmonicity and electron polarization. Use of combined X-ray and neutron data may, however, give problems due to differences in other systematic errors (extinction, absorption, TDS, etc.).

The chemical issues in the $Th(S_2PMe_2)_4$ study center around the role of the 5f electrons in actinide bonding [62], as well as the relative ionic and covalent bonding contributions in actinide and lanthanide complexes [63]. In some theoretical calculations on lanthanides and actinides, it has been found that the bonding contains considerable covalent contributions with significant 5f involvement [64]. The model deformation density in the (0 0 1) plane of $Th(S_2PMe_2)_4$ shown in Fig. 17 reveals a considerable polarization of the Th atom, which is mainly modeled by a contracted set of multipoles on the thorium site (with Tc 4d radial dependence). The Th atom has a depletion of electrons in the *xz* and *yz* contracted d-type orbitals (*x* and *y* directed towards the voids between the ligand atoms) and excess in the contracted $x^2 - y^2$ type orbital. The most important conclusion is that the polarization is mainly of d-symmetry with a radial dependence corresponding to the outer core electrons

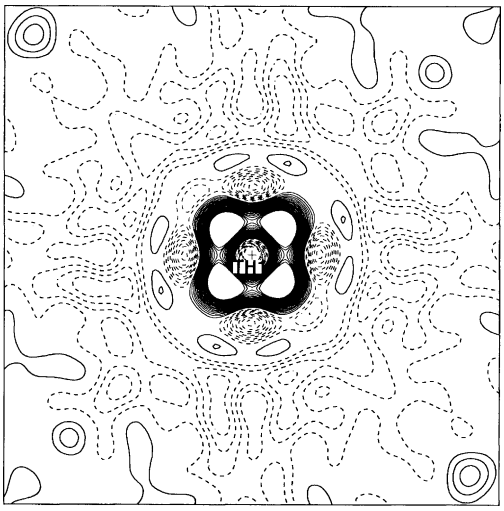

Fig. 17. Dynamic model deformation density of $Th(S_2PMe_2)_4$ in the (0 0 1) plane. The contour interval is 0.1 e $Å^{-3}$. Reprinted with permission from ref. [57a]. Copyright of the American Chemical Society.

(∼5d), and that there is little evidence for diffuse f-type density.

For comparison ab initio calculations were carried out with relativistic core potentials extending to 5d for Th, 2p for S and P and 1s for C. The remaining valence electrons were fitted using a Slater type basis of triple zeta quality. The calculations were not able to reproduce several of the features found in the experiment. First of all theory produced the Th–S bond lengths about 0.2 Å longer than observed, and one of the S–Th–S angles differs by as much as 5°. Secondly, the large polarization observed in the outer Th core could not be reproduced by theory since these electrons were treated with a pseudo potential. Thirdly, the calculations produced a quite covalent bonding picture with considerable 6d–5f mixing. No evidence for covalent bonding was found in the experimental study, and furthermore experimental atomic charges derived from the multipole parameters suggested a quite ionic bonding situation. Overall, the study of $Th(S_2PMe_2)_4$ suggests that theoretical calculations may overestimate the covalent nature of actinide bonding.

4. Synchrotron charge density studies of extended solids

Solids with infinite frameworks formed by metallic, ionic or covalent bonding, or any combination of these pose a special challenge in the experimental charge density field as the unit cells of the often highly symmetric structures tend to be small. Because the scattering pattern is reciprocal to the direct space lattice, being its Fourier transform, this means that the reflections are spaced far apart, and thus that there are very few reflections in the low order region where valence scattering is concentrated. These must be measured with exceptional accuracy if meaningful information is to be obtained. But in normal data collection these reflections

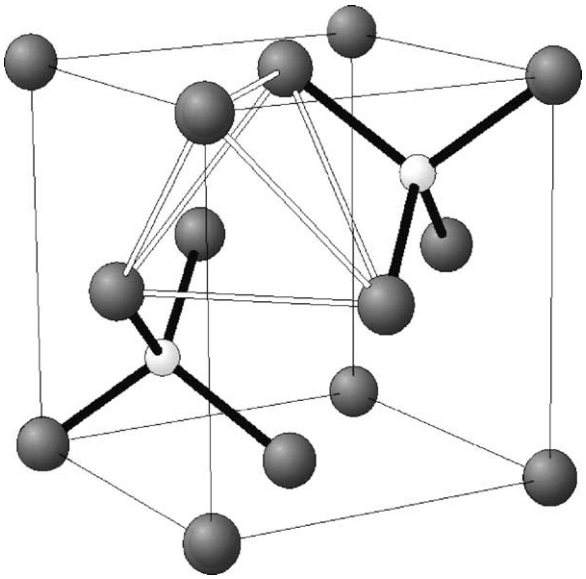

Fig. 18. The cubic structure of Cu_2O. Cu: large gray spheres, O: small white spheres, from reference [83].

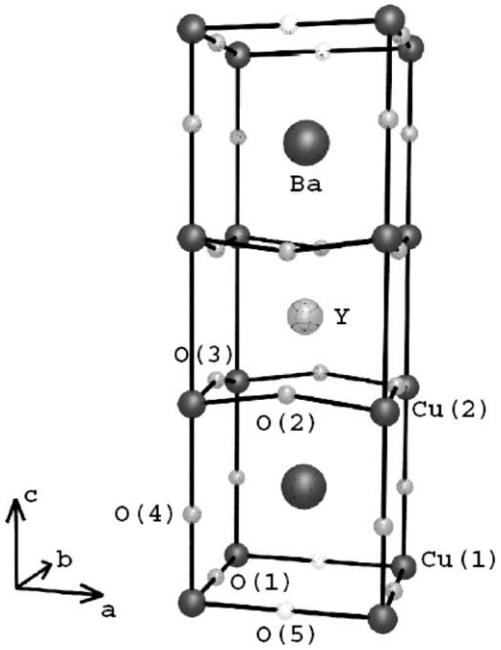

Fig. 19. The structure of $YBa_2Cu_3O_{6.98}$. Y: large bright spheres, Ba: large dark spheres, Cu: small dark sphere and O: small bright spheres, from reference [83].

are also the ones most affected by extinction and multiple scattering effects. Early results obtained in the sixties and seventies are therefore often unreliable. With the advent of synchrotron radiation much smaller crystals can be employed, and most importantly very hard radiation is available, minimizing the parasitic effects, and also allowing extrapolation to zero wavelength if multi-wavelength experiments are performed. A complementary technique, convergent beam electron diffraction (CBED) has recently been used with much success to obtain highly accurate low-order data on a number of solids, which are then combined with conventional higher order data. Pendellösung fringe measurements on perfect crystals have yielded highly accurate structure factors on diamond [65] and especially silicon [66], which have been used to obtain unusually accurate charge densities on these solids. However this technique is limited as perfect or close to perfect crystals must be available.

We will discuss two state-of-the art studies in which the use of synchrotron radiation has been crucial in the elucidation of the nature of the bonding in the solids.

4.1. Cuprite, Cu_2O

The structure of cuprite, Cu_2O is highly symmetrical. It crystallizes in the cubic space group $Pn\bar{3}m$ [$a = 4.2696$ Å, $Z = 2$] with all atoms in special positions [Cu at 000 and equivalent positions, a site with $\bar{3}m$ point symmetry and O at 1/4, 1/4, 1/4, and equivalents, a site with $\bar{4}\,3m$ symmetry] (Fig. 18). In such a situation the intensities of different group of reflections with different even (*e*) or odd (*o*) parity of the three Miller indices characterizing each reflection can vary widely. If the Cu atoms would be truly spherical they would only contribute to the intensities of the strong *eee* and *ooo* group of reflections, while the O atoms would only contribute to the reflections for which the sum of the indices is even, i.e. the *ooe* and *eee* parity groups. Thus, in the hypothetical spherical-atom situation there would be no contribution to the *eeo* parity group of reflections.[2] Nevertheless, such reflections are observed with small but significant intensity and provide detailed information about the anisotropy of the copper atomic vibrations and the chemical bonding.

Restori and Schwarzenbach [67] carefully analyzed Cu_2O with conventional X-ray diffraction data, while Kirfel and Eichhorn [68] carried out a synchrotron experiment using $\lambda = 0.56$ Å radiation. Thus data were available that could be complemented by low-order CBED measurements, as was done by Zuo et al. [69], who obtained an experimental density map with a relatively large (~ 0.2 e Å^{-3}) positive peak in the deformation density at the unoccupied tetrahedral interstitial region of the four neighboring Cu atoms (Fig. 18), suggesting strong Cu^+–Cu^+ covalent bonding.

The deformation density around the copper shows deformation features reminiscent of the d-orbitals depicted in Chemistry text books, which led the authors to conclude that d-orbitals had been observed for the 'first time'. What was in fact observed in this and many earlier studies are deficiencies and excesses in *density* relative to the spherical atom model which is the reference state for the electron deformation density. These can be related to d-orbital populations as reported in the earlier literature, and illustrated above [1,46]. Some of the other conclusions from this study have similarly been questioned [70], leading to extensive discussions [71–73].

[2] A comparable situation exists in other highly symmetric solids such as diamond and V_3Si.

A following study of cuprite by Lippmann et al. used very high-energy synchrotron radiation [74] and was performed at the German synchrotron DESY in Hamburg. Using data measured at 75, 100, 125 and 150 keV (= 0.083 Å) photon energies, it was possible to correct for extinction by extrapolation to zero wavelength and obtain a dataset with excellent internal consistency [74], which gave an unusually good fit in the subsequent multipolar refinements. However, the charge accumulation in the region between the Cu atoms which led to the conclusion of covalent metal–metal bonding was not confirmed in this study, nor was charge accumulation observed between the Cu and O atoms. The detailed topological analysis followed by integration over the atomic basins indicated a charge transfer of about 0.5 e from each of the copper atoms to the oxygen, and gave further evidence for the ionic nature of the bonding in cuprite.

The conclusions of the synchrotron study are supported by quantum-chemical calculations using density functional theory and self-consistent perturbation theory [70,72] which showed a density below 0.08 e Å^{-3} in the interstitial regions between the Cu atoms, in excellent agreement with the experimental synchrotron X-ray value of 0.067(5) e Å^{-3} [74,75].

4.2. Charge density study of a superconducting phase: $YBa_2Cu_3O_{7-x}$

Since the discovery of the high-Tc superconductivity of $YBa_2Cu_3O_{7-x}$ [76] with its relatively high superconducting transition temperature of 90 K several attempts have been made [77–81] to determine the detailed charge density distribution of the solid. The difficulties encountered in the early

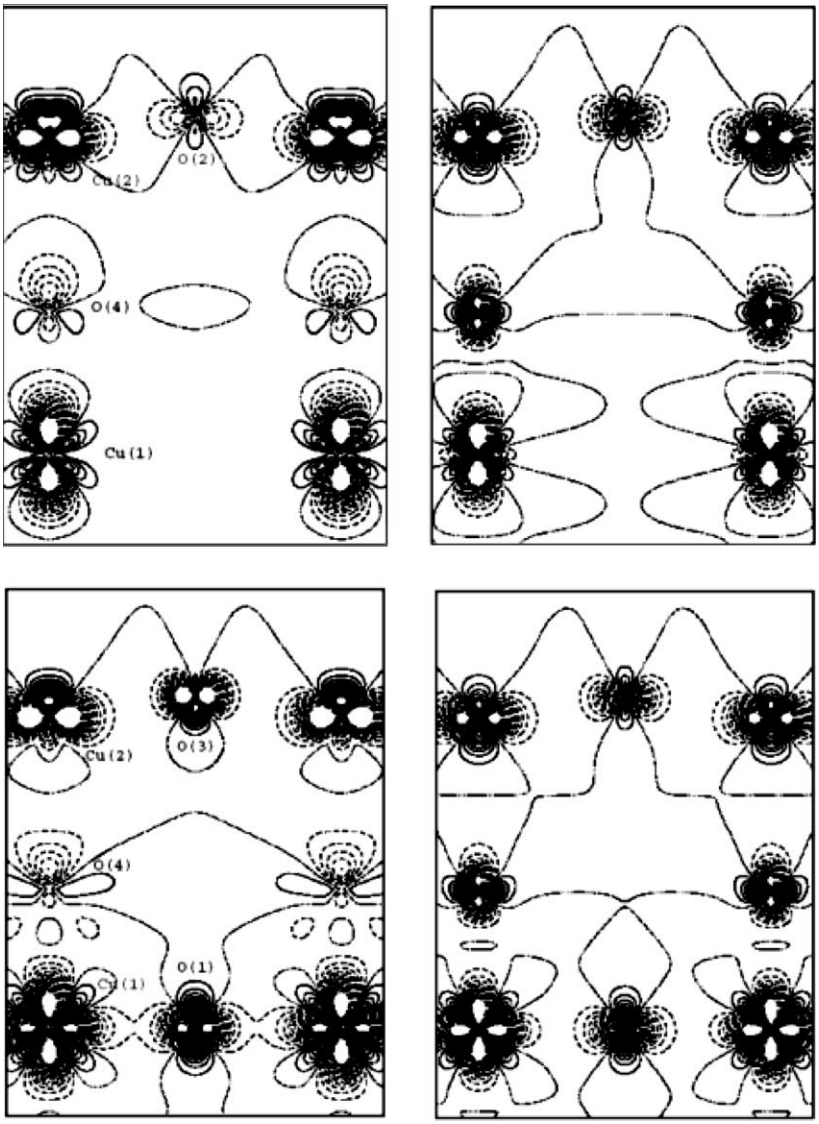

Fig. 20. Electron deformation density in the (0 1 0) (top) and (1 0 0) (bottom) planes of $YBa_2Cu_3O_{6.98}$ Left: From experimental structure factors. Right: From theoretical structure factors based on the APW theoretical density calculated with the Wien2K code. Contours on a geometrical scale starting at 0.0001 e Å^{-3}, and following at 0.0001×2^n. Contours at 0.006 and 0.1 e Å^{-3} dashed, from reference [83].

work are in part related to the low value of 0.016 $Å^3\,e^{-2}$ for the suitability criterion $S = V_{\text{unit cell}}/\sum(N^2_{\text{core}})$ [19] due to the accumulation of many heavy elements in a small unit cell and to the strong extinction and absorption effects encountered in conventional Mo Kα studies of such materials. In addition sample quality presents a difficult handicap. The phase diagram indicates the existence of either a superconducting, orthorhombic or an antiferromagnetic, tetragonal structure depending on the oxygen content *x* of the sample. Growing a mono-domain and un-twinned sample of size, morphology and mosaicity of such a material, suitable for a charge density study is a challenge [82] that can easily interfere with a reliable experimental charge density determination.

A mono-domain tiny crystal with well defined faces was used in a recent charge density analysis of $YBa_2Cu_3O_{6.98}$ [83] performed with high-energy synchrotron radiation of 99.49 keV, λ = 0.124 Å, with which absorption and extinction are very much reduced.

As in the cuprite synchrotron study by the same experimental team, results are compared with density functional theory calculations using the full potential 'Augmented Plane Wave + local orbitals' method as implemented in the Wien2k code [84]. The structure is shown in Fig. 19; the O(5) position at (1/2, 0, 0) is vacant in the $YBa_2Cu_3O_{6.98}$ phase.

Internal consistency between the intensities of equivalent reflections was excellent in this study (with an internal agreement factor of 0.38%). The quality of the data was further tested by structure refinement based on high-order refinement ($\sin\theta/\lambda$ 0.8–1.05 $Å^{-1}$), assuming neutral independent atoms, which gave thermal parameters (often referred to as Atomic Displacement Parameters, ADP) in good agreement with the results of a neutron diffraction study.

Representative deformation density maps in the (0 1 0) and (0 0 1) planes, obtained both with experimental and theoretical structure factors, as shown in Fig. 20. Though the d-orbital populations were not explicitly derived in this study, the deformation maps in this and other planes suggest a redistribution of charge density from the d$[x^2 - y^2]$ orbitals into d_{z^2} orbitals, likely related to the longer Cu(2)–O(4) distance compared to the in-plane Cu–O(3) length. In general orbitals pointing into structural voids such as d$[z^2]$, d[*xy*], d[*xz*] and d[*yz*] orbitals appear to have excess population in agreement with crystal field considerations.

There is both agreement and disagreement between theory and experiment. The densities for Cu(1) and O(1) show pleasing agreement, but the Cu(2) atom appears strongly polarized in the experimental but not in the theoretical density. A similar observation is made for the 'between-planes' oxygen atom O(4). It is interesting that the best of the previous experimental density determinations on this compound by Jang et al. [85] although far from as precise, show some remarkably similar features: no density along the Cu–O bonds, a polarization of Cu(2) with lone pair density accumulation along the *c*-axis on the opposite side of O(4), and a significant deformation density near Ba.

The theoretical results may need further improvement as the Local Density Approximation (LDA) used in the calculation of the density maps does not reproduce the Electric Field Gradient at the Cu(2) site as determined by NQR. On the other hand, the NQR results suggest that the non-spherical densities around O(2) and O(3) must be quite similar, a result not reproduced by the X-ray experiment. Thus, while there is quite good overall agreement between theory and experiment, some of the details differ, which leaves room for further analysis of these important materials.

5. Concluding remarks

At this moment the number of high-accuracy charge density studies on transition metal complexes performed with synchrotron radiation is still limited and the majority of studies reported have been performed at conventional sources [2]. This is likely to change as the compelling advantages of synchrotron radiation will be exploited at the new synchrotron sources now under construction or being planned, and charge density studies are becoming more integrated in chemical research. Especially the application of very high energy synchrotron radiation to extended solids, demonstrated in the last two studies discussed here, has turned the corner in the analysis of extended heavy-atom containing solids, and provides information unsuccessfully sought by use of conventional sources.

The combination of experimental and theoretical methods is an exceptional powerful approach that can point out weaknesses in either method. It is evident that further pursuit of this approach will lead to new insight in the nature of metal–ligand and metal–metal bonding, and in the effect of intermolecular interactions on the electronic structure of molecules in solids.

Acknowledgements

Support of this work by the National Science Foundation (CHE9981864 and CHE0236317), the US Department of Energy (DE-FG02-86ER45231) and the Danish Research Councils (DANSYNC) is gratefully acknowledged.

References

[1] P. Coppens, X-ray Charge Densities and Chemical Bonding, Oxford University Press, 1997.
[2] T.S. Koritsanszky, P. Coppens, Chem. Rev. 101 (2001) 1583.
[3] R.F.W. Bader, Atoms in Molecules: A Quantum Theory, Clarendon Press, 1990.
[4] C.-H. Lee, C.-C. Wang, K.-C. Chen, G.-H. Lee, Y.J. Wang, Phys. Chem. 103 (1999) 156.
[5] G. Gavoille, N.K. Hansen, R. Welter, B. Malaman, H.G. Krane, P. Herzig, J. Phys. Condensed Matter 12 (2000) 2667.
[6] P. Macchi, D.M. Proserpio, A. Sironi, J. Am. Chem. Soc. 120 (1998) 13429.

[7] P. Macchi, L. Garlaschelli, S. Martinengo, A. Sironi, J. Am. Chem. Soc. 121 (1999) 10428.
[8] P. Coppens, G. Wu, A. Volkov, Y. Abramov, Y. Zhang, W.K. Fullagar, L. Ribaud, Trans. Am. Crystallogr. Assoc. 34 (1999) 51.
[9] D.A. Kirzhnits, Sov. Phys. JETP 5 (1957) 64.
[10] Yu.A. Abramov, Acta Crystallogr. A 53 (1997) 264.
[11] V.G. Tsirelson, Acta Crystallogr. B 58 (2002) 632.
[12] E. Espinosa, E. Molins, J. Chem. Phys. 11 (2000) 5686.
[13] P. Macchi, A. Sironi, Coord. Chem. Rev. 238–239 (2003) 383.
[14] R.F. Stewart, J. Chem. Phys. 58 (1973) 1668.
[15] N.K. Hansen, P. Coppens, Acta Crystallogr. A 34 (1978) 909.
[16] T. Koritsanszky, S.T. Howard, T. Richter, P. Macchi, A. Volkov, C. Gatti, P.R. Mallinson, L.J. Farrugia, Z. Su, N.K. Hansen, XD—A Computer Program Package for Multipole Refinement and Topological Analysis of Charge Densities from Diffraction Data, 2003. URL: http://xd.chem.buffalo.edu.
[17] R. Stewart, M. Spackman, C. Flensburg, VALRAY Users Manual, second ed., Department of Chemistry, Carnegie-Mellon University, Pittsburgh, PA 15213, USA and University of Copenhagen, Denmark, 2000.
[18] (a) P. Coppens, A. Holladay, E.D. Stevens, J. Am. Chem. Soc. 104 (1982) 3546;
(b) A. Holladay, P.C. Leung, P. Coppens, Acta Crystallogr. A 39 (1983) 377.
[19] E.D. Stevens, P. Coppens, Acta Crystallogr. A 32 (1976) 915.
[20] B. Schiøtt, J. Overgaard, F.K. Larsen, B.B. Iversen, Int. J. Quan. Chem. 20 (96) (2004) 23.
[21] J. Overgaard, B.B. Iversen, S.P. Palii, G.A. Timco, N.V. Gerbeleu, L. Singerean, F.K. Larsen, Chem. Eur. J. 8 (2002) 2775.
[22] See the entire volume of Chem. Rev. 98 (1998).
[23] See for example Cryst. Eng. Commun. 4 (2002); 5 (2003), especially p. 169.
[24] A. Müller, H. Reuter, S. Dillinger, Angew. Chem. Int. Ed. Engl. 34 (1995) 2328.
[25] M.-M. Rohmer, J. Devémy, R. Wiest, M. Bénard, J. Am. Chem. Soc. 118 (1996) 13007.
[26] J. van Slageren, R. Sessoli, D. Gatteschi, A.A. Smith, M. Helliwell, R.E.P. Winpenny, A. Cornia, A.-L. Barra, A.G.M. Jansen, E. Rentschler, G.A. Timco, Chem. Eur. J. 8 (2002) 277.
[27] B. Rees, A. Mitschler, J. Am. Chem. Soc. 98 (1976) 7918.
[28] S.J. Lippard, Angew. Chem. Int. Ed. Engl. 27 (1988) 344.
[29] J. Limburg, J.S. Vrettos, L.M. Liable-Sands, A.L. Rheingold, R.H. Crabtree, G.W. Brudvig, Science 283 (1999) 1524.
[30] R.D. Cannon, R.P. White, Prog. Inorg. Chem. 36 (1988) 195.
[31] (a) G. Wu, Y. Zhang, L. Ribaud, P. Coppens, C. Wilson, B.B. Iversen, F.K. Larsen, Inorg. Chem. 37 (1998) 6078;
(b) C. Wilson, B.B. Iversen, F.K. Larsen, J. Overgaard, G. Wu, S.P. Palii, G.A. Timco, N.V. Gerbeleu, J. Am. Chem Soc. 122 (2000) 11370;
(c) S.P. Palii, G.A. Timco, N.V. Gerbeleu, M.L. Hansen, B.B. Iversen, F.K. Larsen, Inorg. Chim. Acta (2001) 23.
[32] J. Overgaard, F.K. Larsen, B. Schiøtt, B.B. Iversen, J. Am. Chem. Soc. 125 (2003) 11088.
[33] B.L. Rodrigues, G. Wu, P. Coppens, in press.
[34] M.J. Frisch, G.W. Trucks, H.B. Schlegel, G.E. Scuseria, M.A. Robb, J.R. Cheeseman, V.G. Zakrzewski, J.A. Montgomery Jr., R.E. Stratmann, J.C. Burant, S. Dapprich, J.M. Millam, A.D. Daniels, K.N. Kudin, M.C. Strain, O. Farkas, J. Tomasi, V. Barone, M. Cossi, R. Cammi, B. Mennucci, C. Pomelli, C. Adamo, S. Clifford, J. Ochterski, G.A. Petersson, P.Y. Ayala, Q. Cui, K. Morokuma, D.K. Malick, A.D. Rabuck, K. Raghavachari, J.B. Foresman, J. Cioslowski, J.V. Ortiz, A.G. Baboul, B.B. Stefanov, G. Liu, A. Liashenko, P. Piskorz, I. Komaromi, R. Gomperts, R.L. Martin, D.J. Fox, T. Keith, M.A. Al-Laham, C.Y. Peng, A. Nanayakkara, C. Gonzalez, M. Challacombe, P.M.W. Gill, B.G. Johnson, W. Chen, M.W. Wong, J.L. Andres, M. Head-Gordon, E.S. Replogle, J.A. Pople, Gaussian 98, Gaussian Inc., Pittsburgh, PA, 1998.
[35] R.D. Ernst, Comments Inorg. Chem. 21 (1999) 285.
[36] I. Hyla-Kryspin, T.E. Waldman, E. Melendez, W. Trakarnpruk, A.M. Arif, M.L. Ziegler, R.D. Ernst, R. Gleiter, Organometallics 14 (1995) 5030.
[37] A.M. Wilson, F.G. West, A.L. Rheingold, R.D. Ernst, Inorg. Chim. Acta 300–302 (2000) 65.
[38] V. Kulsomphob, B.G. Harvey, A.M. Arif, R.D. Ernst, Inorg. Chim. Acta 334 (2002) 17.
[39] R. Tomaszewski, I. Hyla-Kryspin, C.L. Mayne, A.M. Arif, R. Gleiter, R.D. Ernst, J. Am. Chem. Soc. 120 (1998) 2959.
[40] R. Tomaszewski, K.-C. Lam, A.L. Rheingold, R.D. Ernst, Organometallics 18 (1999) 4174.
[41] G.J. Kubas, C.J. Unkefer, B.I. Swanson, E. Fukushima, J. Am. Chem. Soc. 108 (1986) 7000.
[42] G.J. Kubas, Metal Dihydrogen and σ-Bond Complexes, Kluwer Academic Publishers/Plenum Press, New York, 2001.
[43] S.S. Stahl, J.A. Labinger, J.E. Bercaw, Inorg. Chem. 37 (1998) 2422.
[44] W. Scherer, W. Hieringer, M. Spiegler, P. Sirsch, G.S. McGrady, A.J. Downs, A. Haaland, B. Pedersen, Chem. Commun. (1998) 2471.
[45] S. Pillet, G. Wu, V. Kulsomphob, B.G. Harvey, R.D. Ernst, P. Coppens, J. Am. Chem. Soc. 125 (2003) 1937.
[46] A. Holladay, P. Leung, P. Coppens, Acta Crystallogr. A 39 (1983) 377.
[47] R.F.W. Bader, C.F. Matta, Inorg. Chem. 40 (2001) 5603.
[48] P.L.A. Popelier, G. Logothetis, J. Organomet. Chem. 555 (1998) 101.
[49] R.H. Crabtree, E.M. Holt, M. Lavin, S.M. Morehouse, Inorg. Chem. 24 (1985) 1986.
[50] P. Macchi, A.J. Schultz, F.K. Larsen, B.B. Iversen, J. Phys. Chem. 105 (2001) 9231.
[51] (a) P.E.M. Siegbahn, J. Phys. Chem. 97 (1993) 9096;
(b) I. Bytheway, M.B. Hall, Chem. Rev. 94 (1994) 639.
[52] K.A. Jørgensen, Chem. Rev. 89 (1989) 431.
[53] (a) D.V. Deubel, J. Sundermeyer, G. Frenking, J. Am. Chem. Soc. 122 (2000) 10101;
(b) J.M. Michell, N.S. Finney, J. Am. Chem. Soc. 123 (2001) 862.
[54] (a) H. Mimoun, I. Seree de Roch, L. Sajus, Tetrahedron 26 (1970) 37;
(b) H. Mimoun, Angew. Chem. 21 (1982) 734.
[55] K.B. Sharpless, J.M. Townsend, D.R. Williams, J. Am. Chem. Soc. 94 (1972) 295.
[56] O. Eisenstein, R. Hoffmann, J. Am. Chem. Soc. 103 (1981) 4308.
[57] (a) B.B. Iversen, F.K. Larsen, A.A. Pinkerton, A. Martin, A. Darovsky, P.A. Reynolds, Inorg. Chem. 37 (1998) 4559;
(b) B.B. Iversen, F.K. Larsen, A.A. Pinkerton, A. Martin, A. Darovsky, P.A. Reynolds, Acta Crystallogr. B 55 (1999) 363.
[58] A. Darovsky, R. Bolotovsky, P. Coppens, J. Appl. Cryst. 27 (1994) 1039.
[59] A.A. Pinkerton, A.E. Storey, J.M. Zellweger, J. Chem. Soc., Dalton Trans. (1981) 1475.
[60] R. Restori, D. Schwarzenbach, Acta Crystallogr. A 52 (1996) 369.
[61] P.R. Mallinson, T. Koritsanszky, E. Elkaim, N. Li, P. Coppens, Acta Crystallogr. A 44 (1988) 336.
[62] B.E. Bursten, R.J. Strittmatter, Angew. Chem. Int. Ed. 30 (1991) 1069.
[63] C. Adamo, P. Maldivi, Chem. Phys. Lett. 61 (1997) 61.
[64] A.A.H. Chang, R.M. Pitzer, J. Am. Chem. Soc. 111 (1989) 2500.
[65] T. Takama, K. Tsuchiya, K. Kobayashi, S. Sato, Acta Cryst. A46 (1990) 514.
[66] S. Tanemura, N. Kato, Acta Cryst. A28 (1972) 69;
P.J.E. Aldred, M. Hart, Proc. R. Soc. Lond. Ser. A 332 (1973) 223;
T. Saka, N. Kato, Acta Cryst. A43 (1987) 252.
[67] R. Restori, D. Schwarzenbach, Acta Crystallogr. B 42 (1986) 201.
[68] A. Kirfel, K. Eichhorn, Acta Crystallogr. A 46 (1990) 271.
[69] J.M. Zuo, M. Kim, M. O'Keeffe, J.C.H. Spence, Nature (1999) 401.
[70] S.-G. Wang, W.H.E. Schwarz, Angew. Chem. Int. Ed. Engl. 39 (2000) 1757.

[71] J.M. Zuo, M. O'Keeffe, M. Kim, J.C.H. Spence, Angew. Chem. Int. Ed. Engl. 39 (2000) 3791.
[72] S.G. Wang, W.H.E. Schwarz, Angew. Chem. Int. Ed. Engl. 39 (2000) 3794.
[73] E.J. Scerri, J. Chem. Ed. 77 (2000) 1492.
[74] T. Lippmann, J.R. Schneider, J. Appl. Crystallogr. 33 (2000) 156.
[75] T. Lippmann, J.R. Schneider, Acta Crystallogr. A 56 (2000) 575.
[76] M.K. Wu, J.R. Ashburm, C.J. Torng, P.H. Hor, R.L. Meng, L. Gao, Z.J. Huang, Y.Q. Wang, C.W. Chu, Phys. Rev. Lett. 58 (1987) 908.
[77] S. Sasaki, Z. Inoue, N. Iyi, S. Takekawa, Acta Crystallogr. B 48 (1992) 393.
[78] R. Buttner, E. Maslen, Acta Crystallogr. B 48 (1992) 644.
[79] R. Buttner, E. Maslen, N. Spadaccini, Acta Crystallogr. B 48 (1992) 21.
[80] J. Sullivan, P. Bordet, M. Marezio, K. Takenaka, S. Uchida, Phys. Rev. B 48 (1993) 10638.
[81] W.-J. Jang, H. Mori, M. Watahiki, S. Tajima, N. Koshizuka, S. Tanaka, J. Solid State Chem. 122 (1996) 371.
[82] T. Wolf, J. Cryst. Growth 166 (1996) 810.
[83] T. Lippmann, P. Blaha, N.H. Andersen, H.F. Poulsen, T. Wolf, J.R. Schneider, K.H. Schwarz, Acta Crystallogr. A 59 (2003) 437–451.
[84] P. Blaha, K. Schwarz, G. Madsen, D. Kvasnicka, J. Luitz, WIEN2k: An Augmented Plane Wave + Local Orbitals Program for Calculating Crystal Properties, K. Schwarz, Technische Universität Wien, Austria, 2001, ISBN 3-9501031-1-2.
[85] W.-J. Jang, H. Mori, M. Watahiki, S. Tajima, N. Koshizuka, S. Tanaka, J. Solid State Chem. 122 (1996) 371.